



The Spectral Characterization of Novel Spacecraft Materials in the Low Earth Orbit Environment

Elena A. Plis^{1,2}  · Gregory Badura¹

Accepted: 25 January 2024 / Published online: 8 March 2024
© The Author(s), under exclusive licence to American Astronautical Society 2024

Abstract

The protection of satellites from the harsh space environment is heavily reliant on external spacecraft materials. These materials undergo continuous changes in their physical, chemical, and optical properties due to exposure to solar radiation and aggressive chemical species present in Earth's upper atmosphere. By gaining a thorough understanding of how these material properties evolve over the planned lifetime of a mission, the reliability of spacecraft can be enhanced. Additionally, the establishment of correlation factors between actual space exposure and accelerated space weather experiments performed in ground facilities allows for the precise prediction of on-orbit material performance based on laboratory-based testing. This paper presents an assessment of the radiation effects of the low Earth orbit environment, including exposure to high-energy electrons, atomic oxygen, and vacuum ultraviolet, on the material properties of a prospective spacecraft polymer, Mylar® M021. The study is part of the 16th Materials International Space Station Experiment (MISSE), which our team conducted from 08/31/22 to 02/23/23. An overview of the MISSE project is provided, including details on the materials used, results of ground experiments, and preliminary findings from the orbital phase of the study.

Keywords Low Earth orbit · MISSE · Electron irradiation · Atomic oxygen exposure · Vacuum ultraviolet exposure

1 Introduction

The low Earth orbit (LEO) is a valuable asset of humankind for many different reasons. LEO satellites have been utilized for voice and data communication since 1998 (Iridium Communications Inc.'s network) due to the low delay that occurs in

✉ Elena A. Plis
elena.plis@gtri.gatech.edu

¹ Georgia Tech Research Institute, 925 Dalney St NW, Atlanta, GA 30318, USA

² Assurance Technology Corporation, Carlisle, MA 01741, USA

round-trip data transmission. Since then, the number of communication satellites in LEO has increased significantly, with over 3,717 Starlink satellites launched since 2018 to provide high-speed internet service worldwide [1]. These satellite surveillance and communication capabilities are vital for USSF military and intelligence operations. Next, LEO is a critical staging point for space exploration and the development of technologies required for future missions to more distant destinations such as the Moon, Mars, and beyond. Finally, humankind's only permanent residence in space, the International Space Station (ISS), is operating in LEO.

During a space mission, surface spacecraft materials are exposed to various environmental factors such as different types of ionizing radiation, including high-energy electrons and protons, AO ions, micrometeoroids, vacuum, and large temperature fluctuations [2–4]. The resulting change in the material properties can significantly impact materials' performance and durability [e.g., 5, 6] which could degrade the functionality of the spacecraft elements. Even though all space environmental components can lead to the deterioration of spacecraft components, the threat posed by AO, the most abundant specie at LEO, is especially severe in terms of structural, thermal, and optical damage, particularly to exterior spacecraft components that are susceptible to oxidation [7].

A comprehensive understanding of how the properties of materials change over the course of a long-term space mission is crucial for ensuring that the materials used can withstand the harsh conditions of space and function as intended throughout the mission. Moreover, as space exploration becomes simultaneously more commonplace and ambitious, new and advanced materials are required to meet the increasingly demanding needs of space missions. Novel materials born on the expanding boundaries of organic polymer chemistry must be lightweight, have improved long-term radiation shielding properties, and possess improved mechanical properties such as enhanced elasticity and mechanical strength for use in internal and external spacecraft systems.

One major barrier to utilizing novel materials on spacecraft is the immense cost of flying to space. Testing novel materials intended for the spacecraft industry on Earth may be difficult, as it is challenging to recreate the exact space environment in a laboratory setting. LEO is a particularly harsh environment for organic polymers because AO is present along with all other environmental components [8]. Efforts to reproduce the complex LEO environment in ground-based facilities have been reported by US and international research teams [e.g., 9–11]. However, significant differences exist between actual LEO and ground-based exposures (i.e., variations in AO quantum state and AO energies and fluxes, temperature cycling, and simultaneous UV and ionizing radiation). In addition, the effects of the space environment on spacecraft components vary based on specific mission details such as mission duration, orbital parameters, view angle of spacecraft surfaces to the sun, and orientation of spacecraft surfaces with respect to the spacecraft velocity vector in LEO [12]. Such integrated testing with replication of actual space conditions is virtually impossible to realize in Earth-based testing facilities. Therefore, ground-based experiments must be benchmarked against actual LEO exposure. The MISSE flight facility (MISSE-FF) provides unique capabilities for testing neoteric materials under exposure to the integrated space environment. Establishing correlation factors between actual space exposure and accelerated space

weather experiments is a key benefit of using the MISSE-FF in conjunction with space-simulated facilities. This enables accurate prediction of on-orbit material performance based on laboratory-based testing, which can improve the reliability and safety of space missions.

The MISSE project is a NASA initiative that was launched in 2001 with the aim of studying the effects of the LEO space environment on a variety of materials. Since its inception, the MISSE project has tested approximately 4,000 different material samples and specimens, evaluating their durability and performance in the harsh and challenging conditions of space. From 2001 to 2013, individual flight experiments were carried out using Passive Experiment Containers (PECs), which were suitcase-like containers placed outside the ISS either in a Ram/Wake or a Zenith/Nadir orientation by an astronaut during a spacewalk [13]. Following the 1-4 years exposure period, the PECs were retrieved during a spacewalk and brought back to Earth on the shuttle for post-flight analysis. In 2018, the MISSE-FF, a modular robotically serviceable external platform that can be configured to carry out a wide range of passive and active experiments, was launched [14]. Since then, several ~6 months long MISSE missions were successfully completed.

The project discussed here was a component of the MISSE-16 space mission, which was launched aboard the SpaceX-25 spacecraft from Kennedy Space Center on July 15th, 2022, and subsequently docked at the Harmony Forward (Node 2 Forward) on July 16th, 2022. MISSE-16 Science Carriers (MSCs) were installed on the MISSE-FF on 31 July–2 August 2022 with support from the Canada Space Agency ISS Robotic Systems Team.

This project aimed to gather high-fidelity time-resolved spectral measurements along with environmental data collected at the same cadence in order to clearly delineate the effect of total irradiation dose as well as any flux-dependent material response. During the expected mission duration (approx. 6 months), we intend to investigate short- and long-term degradation effects of LEO on selected materials, by tracking their spectral properties as a function of time-on-orbit. Previous experiments have shown that radiation-induced color change occurs rapidly upon first exposure to radiation and that the changes become more gradual with increasing fluence. By correlating color change to a host of other material properties determined using ground-based characterization, we will enable Earth-bound observers to remotely diagnose spacecraft health based on color shifts detected via unresolved remote observations. Lastly, laboratory-based irradiation experiments are nearly always performed at an accelerated dose rate with imperfect radiation sources. Therefore, truth data gathered in the real space weather environment is invaluable for developing accurate ground testing protocols.

This paper offers a high-level overview of the project, including details on the materials used, results of ground experiments, and preliminary findings from the orbital phase of the study.

2 Experimental Procedure

2.1 Materials

Three identical sets of samples were placed on the Ram, Zenith, and Wake faces of the ISS. Table 1 lists the flight samples that included several materials from the Kapton® family, polyethylene terephthalate (PET), liquid crystal polymer (LCP), carbon and glass fiber-reinforced polymers (CFRP and GFRP, respectively), polyhedral oligomeric silsesquioxanes (POSS), and alumina slide. The area of each sample was 1 inch². The samples were constructed by stacking multiple layers to achieve a minimum total thickness of 10 mils (0.01 inch). In some cases, more than one layer was required to reach the desired thickness. For space-simulated experiments including exposure to AO, VUV, and high-energy electrons, single-layer samples were utilized.

Kapton® has been a trusted material for safeguarding satellites, spacecraft, and astronauts for over five decades, dating back to the Apollo 11 mission [15]. We used Kapton-HN® film as a well-established reference material for our experiments. Furthermore, we incorporated various new Kapton formulations, including CR (corona-resistant, crucial for shielding sensitive equipment on spacecraft), CS (clear, smooth, and thermoformable, with potential to replace traditional PI film in MLI blankets and enhance next-generation space solar cells), WS (opaque film with high thermal stability, a viable alternative to traditional PI film in MLI blankets), XC (electrically conductive, valuable for mitigating space charge on spacecraft), and TF

Table 1 List of materials for flight samples

	Material/tradename	Abbreviation	Density (g/cm ³)	Single layer thickness (mil)	# of layers	MSC side
1	Kapton® CR	Polyimide (PI)	1.54	2	5	Mount
2	Kapton® CS		1.42	2	5	
3	Kapton® WS		1.42	1	10	
4	Kapton® XC		1.41	2	5	
5	Kapton® TF		1.42	4	3	
6	DR9		1.42	2	5	
7	Kapton® HN		1.43	3	4	
8	Economyplate™ Carbon Fiber	CFRP	1.44	29	1	
9	G-10/FR4 Glass Epoxy	GFRP	1.90	66	1	
10	Zenite®	LCP	1.75	3	4	
11	Melinex® 454	PET	1.20	5	2	
12	Mylar® M021		1.39	9	1	Swing
13	CORIN® XLS	POSS	1.40	0.6	17	
14	Thermalbright® N		2.08	0.8	13	
15	Alumina	ALUM	3.95	3.8	3	

(thermoformable, a promising material for small satellite components). Additionally, we flew the DR9 polymer, a novel high-performance organic polymer material that has not been previously tested for spacecraft applications.

CFRP and GFRP are widely used in the construction of present-day LEO satellites [16, 17]. Unfortunately, little is known about the evolution of the optical properties of these materials in the harsh LEO environment [18, 19]. Laboratory impact tests have shown that CFRP shatters into small needle-like shapes, which are a clear risk in the orbital debris environment. It is unclear whether the optical properties of these fragments change following impact, complicating ground-based observations of these objects. GFRP tends to be translucent in nature and laboratory studies have not determined how or if it degrades with time-on-orbit. Studying the optical properties of these materials would provide a baseline of how they respond to the harsh LEO environment and allow better monitoring for improved space domain awareness.

LCPs present a special category of materials, which straddles the boundary between an ordinary solid and a liquid. LCPs have excellent dimensional stability (fatigue and creep resistance), as well as high dielectric strength over wide temperature range [20]. Moreover, LCPs show a high resistance to UV radiation and very good electrical insulation properties [21]. These unique properties in conjunction with light weight make LCP materials very attractive for space applications. Flexible LCP antennas and LCP-based circuits molded to available spacecraft areas could eliminate heavy metal boxes that currently house rigid circuit boards [22]. Before recommendation of LCP material to spacecraft designers, evaluation of its durability under the harsh space conditions of LEO must be performed. We will test effect of LEO environment on one variety of DuPont Zenite® LCP.

PET films are an essential part of multi-layer insulation (MLI) blankets that are used on the exterior surfaces of spacecraft for the purpose of passive thermal control. MLI composite materials work by limiting the amount of radiative heat transfer through multiple layers of thin reflectors (shields) and spacer materials. The shields are generally PET or polyimide (PI) metal-coated films with high mechanical strength and low thermal conductivity. An ideal thermal blanket completely reflects the incident radiation. Although these perfect reflectance characteristics have not been obtainable in practice yet [23] and research is being conducted on alternatives to traditional MLI blankets, such as those based on silica aerogels [24–26], which offer improved reflectivity and durability, PET-based shields are still an essential part of spacecraft thermal control system. Thus, new materials need to be developed for improved MLI reflectivity and durability. We included two novel types of PET, Melinex® 454 and Mylar® MO21, into the experimental materials selection.

One promising method to increase the AO-resistivity of PI films is incorporation of the monomer POSS into the PI polymer matrix, either as a chemically bound co-polymer or an additive blended into the matrix [5, 6]. The unique benefit of this method over traditional methods, such as coatings, is that when POSS-PI is initially exposed to AO, it forms a layer of SiO_x over the surface. This passivating layer prevents further material ablation, thus lowering the overall erosion yield. Moreover, if the surface is damaged in anyway and cracks appear, the newly exposed surface will simply form another layer of SiO_x. Hence, POSS-PI essentially a self-healing

polymer. We included two POSS/PI samples, Thermalbright™ (a colorless polyimide with POSS additives) and CORIN® (a transparent, sprayable PI with POSS additives). As PI/POSS hybrid materials have already been identified as excellent AO resistant materials, a detailed study of their optical properties will be of great utility to the remote sensing community for the characterization of orbital debris and operational RSOs.

Finally, to ensure the accurate comparison between images captured after different space exposure times, we have chosen pure aluminum oxide (alumina, Al_2O_3) as our reflectance standard as it is resistant to AO attack and has a flat white spectral profile.

2.2 Space-Simulated Irradiation Procedure

Material irradiation with high-energy electrons as well as the VUV exposure was performed in the Jumbo space irradiation chamber at the Spacecraft Charging and Instrument Calibration Laboratory (SCICL) at Kirtland AFRL [27]. Materials were bombarded with high-energy (100 keV) electrons produced by a mono-energetic Kimball Physics EG8105-UD electron flood gun. The maximum electron fluence the materials under investigation were exposed to is 8.5×10^{13} electrons/cm², which corresponds to approximately 10 years at 600–800 km (LEO) orbit, delivered during 5.5 h. A 24-h vacuum dehydration bakeout was performed on all samples at 60° C prior to radiation exposure to remove any absorbed water. Details of the electron irradiation procedure are reported elsewhere [28].

The space-simulated VUV exposure was conducted using three Resonance KrLM-LQD12 lamps installed in the Jumbo chamber at SCICL. The lamp spectrum is composed of 1.0 parts and 2.38 parts of photons with peak wavelengths at 116.5 nm and 123.6 nm, respectively [29]. The photon flux at each wavelength was estimated as 5.5×10^{20} photons/ (seconds · cm² · Å) at 116.5 nm and 1.06×10^{20} photons/ (seconds · cm² · Å) at 123.6 nm. Based on Lyman-Alpha flux in-vacuum conversion [30], samples receive an average of 50.9 equivalent sun hours (ESH) per single sample carousel rotation. The expected solar net flux for 6 months of the MISSE-16 mission was calculated to be ~1094 ESH, assuming that ISS completes approximately sixteen 90-min revolutions per day. Samples studied in this work were exposed to ~6 months of LEO space weather in ~23 h.

Exposure testing of sample materials to an 8 km/s oxygen atom beam was conducted according to ASTM-E2089-15A using the FAST source at the Physical Sciences Inc. The effective peak atomic oxygen fluence during the exposure was calculated using the known witness sample density (Kapton® H, 1.427 g/cm³) and LEO erosion yield of the same material (3×10^{-24} cm³/O-atom). Effective peak atomic oxygen fluence during the run was 3.1×10^{20} O-atom/cm² which corresponds to 6 weeks of LEO exposure. Prior to exposure, all samples were stored in the vacuum chamber for 24 h to remove water. They were then evacuated and weighed over time to monitor water absorption and allow for the dry mass calculation. Details of the AO-irradiation procedure may be found in [31].

2.3 Orbital Irradiation Experiments

The LEO exposure time of each MSCs is presented in Table 2.

Upon reviewing the radiation data for MISSE-16, the Aegis Aerospace operations team observed that the data may have been affected by noise in the active radiation sensor. Consequently, the team has decided to wait for the passive dosimeter data to become available. These data will be acquired after the MISSE science carriers are retrieved and processed by the dosimeter manufacturer. This will enable our team to obtain more accurate radiation measurements and mitigate the effects of any potential noise in the active radiation sensor data.

2.4 Characterization Protocol for Flight Duplicate Materials

As part of the characterization process, several different measurements were conducted to assess the properties of the test samples, with a focus on their optical characteristics. Optical measurements were performed using techniques such as direct hemispherical reflectance (DHR), reflectance (R), transmittance (T), Fourier-transform infrared spectroscopy (FTIR), and bidirectional reflectance distribution function (BRDF) measurements. In addition, surface morphology characterization was undertaken using scanning electron microscopy (SEM) and atomic force microscopy (AFM). To access the changes in radiation-induced electrical conductivity of the materials, surface potential decay (SPD) [32] and ASTM-D-257 techniques were employed. Finally, visible and infrared (IR) images of all radiation-damaged materials were taken *in vacuo* using the same Basler daA1600 camera and illumination scheme as was utilized in MSCs.

AFM measurements were performed using Bruker Dimension ICON instrument allowing measurement of surface roughness up to 5 μm on areas as large as 200 $\mu\text{m} \times 200 \mu\text{m}$. SEM measurements were performed using Hitachi SU-8230 which features novel cold field emission (CFE) gun for improved imaging and analytical performance.

The DHR measurements were performed in accordance with the optical data acquisition procedure reported elsewhere [33]. UV/Vis transmission measurements were performed with the Cary 5000 UV–Vis–NIR spectrometer. The Hemispherical Conical Reflectance Factor (HCRF), the laboratory approximation of true Bidirectional Reflectance Distribution Function (BRDF) measurements, of pristine samples with fixed viewing angles (0°, 30°, 60°, – 30°, and – 60°) and variable illumination angles (0°–70° degrees range, exact values of illumination angles are specified separately for each measurement), was evaluated in the principal plane of illumination.

Table 2 MSCs exposure times

MSC	Exposure time
Wake	193 days \approx 6.3 months
Zenith	194 days \approx 6.3 months
Ram	183 days \approx 6.0 months

The samples were illuminated with a collimated 50 Watt tungsten halogen that approximated a blackbody source over the range of 350–2500 nm. An Analytical Spectral Devices Spectrometer was used to collect radiance measurements over this spectral range [34]. FTIR measurements were performed with Nicolet 6700 FT-IR spectrometers from Thermo Electron Corporation, with a wavenumber resolution of 2 nm. For reflectance measurements, an Analytical Spectral Device (ASD) field spectrometer, ASD FieldSpec4, with a range from 300 to 2500 nm and a full-width half maximum of 3 nm at 700 nm, and 10 nm at 1400/2100 nm, respectively, was employed. In addition, mass loss of AO-exposed materials was measured with 10 μ g accuracy using the microgram balance and then AO-erosion rate was estimated.

Geographically, the members of the research team are separated by hundreds of miles. In particular, the electron and UV space-simulated exposure was performed at the SCICL laboratory whereas AO exposure was outsourced to Physical Sciences Inc [35] (Fig. 1). Some of the characterizations of the space weather effects on material properties of spacecraft materials were in situ at the SCICL and, mainly, ex situ at the GTRI. To ensure the accuracy of the characterization experiments, it is important to guarantee that all collaborators receive space-weather-exposed samples that have undergone minimal recovery from their atmospheric exposure, and that all characterization procedures are carried out with minimal air exposure. To comply with these requirements, we have developed a procedure for handling spacecraft materials that are sensitive to atmospheric exposure [36]. This procedure allows sufficient time for the delivery of air-sensitive materials and for conducting all intended characterization experiments on radiation-damaged materials.

2.5 Characterization Protocol for Flight Materials

Visible and IR images of every sample were sequentially acquired using a Basler daA1600 camera on MSCs mounted on zenith, ram, and wake ISS faces. The experimental cadence includes daily images during the first week of the materials' exposure, weekly during the next two months, and monthly till the end of the mission. It

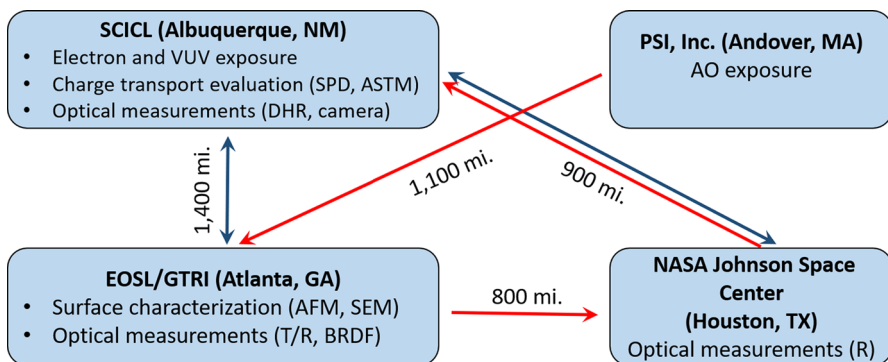


Fig. 1 Transfer logistics of spacecraft materials exposed to the space-simulated environments. The blue lines correspond to the transfer of electron-irradiated and VUV-exposed samples, the red lines correspond to the transfer of AO-exposed materials

should be noted that there was a sensor anomaly that prevented AEGIS Aerospace from fully opening the swing side of wake and ram MSCs. Thus, data collection was not performed for the four samples, namely, #12 (Mylar® M021), #13 (CORIN XLS), #14 (Thermalbright® N), and #15 (Alumina), placed on the swing side of ram and wake MSCs. Our team will have the chance to examine all of the materials after they return to Earth, so for these particular samples at least two data points will be obtained, namely, at their pristine state (taken on Earth prior to the mission) and at the most damaged state (to be taken again on Earth after MISSE- FF comes back on April'23).

Optical images were downlinked to Earth within days of the performed measurements. After initial analysis of those images, a machine learning (ML) approach based on a radial basis function (RBF) network [37] was utilized to extract reflectance spectra from RGB/IR images. Once images are downloaded from the on-orbit MISSE-FF cameras, the RGB data are selected from non-oversaturated regions under both visible and IR lighting conditions. Next, these pixel counts were white-balanced given the scene context, which is possible because the same settings have been applied to the flight and ground cameras. Finally, the RGB MISSE-FF data were converted into the $L^*a^*b^*$ color space and fed into the RBF network. The ML algorithm produced an estimated reflectance spectrum for each image. A summary of the approach utilizing ML and computer vision algorithms to retrieve reflectance data from RGB images is shown in Fig. 2.

3 Results

Due to the abundance of samples in our study, it is not feasible to present the results for all materials. Therefore, we will focus our discussion on one particular material, namely, Mylar® M021. Table 3 summarizes the surface roughness of pristine, electron-irradiated, AO- and VUV-exposed Mylar® M021 accessed by AFM. Average surface roughness (Ra) values are averages of several $5 \mu\text{m} \times 5 \mu\text{m}$ scans taken at different parts of the sample. Representative $5 \mu\text{m} \times 5 \mu\text{m}$ AFM scans of pristine

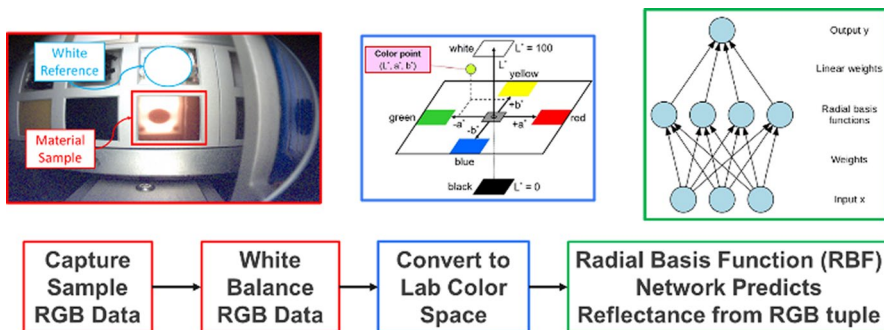


Fig. 2 Summary of approach utilizing ML and computer vision algorithms to retrieve reflectance data from RGB images

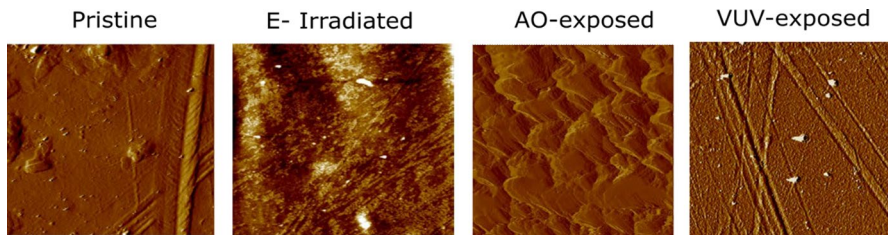
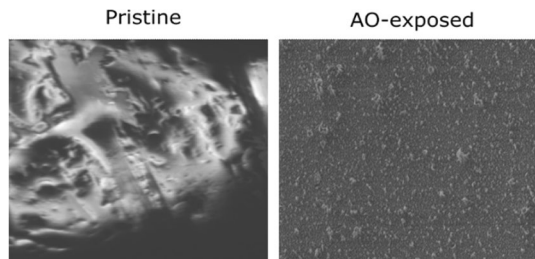
Table 3 Surface roughness of Mylar® M021 exposed to different components of space-simulated environment

Pristine	Electron-irradiated	AO-exposed	VUV-exposed
7.8 nm	3.6 nm	187.2 nm	4.6 nm

and exposed to different components of space-simulated environment Mylar® M021 material are shown in Fig. 3. Since no significant effect of electron and VUV exposure on the surface roughness of the material was observed, whereas AO exposure significantly affected the material's morphology, SEM images of only AO-exposed Mylar® M021 samples were taken, as shown in Fig. 4.

Mass loss, erosion rate, and relative erosion rate with respect to the Kapton® HN of the 9 mil Mylar® M021 sample after AO exposure was 7.89 mg, 7.29×10^{-21} g/cm²/O-atom, and 1.70, respectively.

Figure 5 presents the DHR spectra of control (pristine), electron-irradiated, and VUV-exposed Mylar® M021 material in 400–2000 nm spectral range taken at different levels of space-simulated exposure. Since AO irradiation was performed at a different facility, no DHR data were taken for the AO-exposed material. Comparison of transmission characteristics (within 200 – 2000 nm wavelength range) of pristine and exposed to the different components of the space-simulated weather Mylar® M021 is presented in Fig. 6. The respective FTIR transmission curves are shown in Fig. 7. Representative HCFR data which were taken at one selected pair of viewing and illumination angles ($\Theta_i = 0^\circ$ and $\Theta_v = 30^\circ$) is presented in Fig. 8. The absolute reflectance measurements were performed for all

**Fig. 3** Representative 5 $\mu\text{m} \times 5 \mu\text{m}$ AFM scans of pristine, electron-irradiated, AO-exposed, and VUV-exposed Mylar® M021**Fig. 4** Representative 200 $\mu\text{m} \times 200 \mu\text{m}$ SEM images of pristine and AO-exposed Mylar® M021

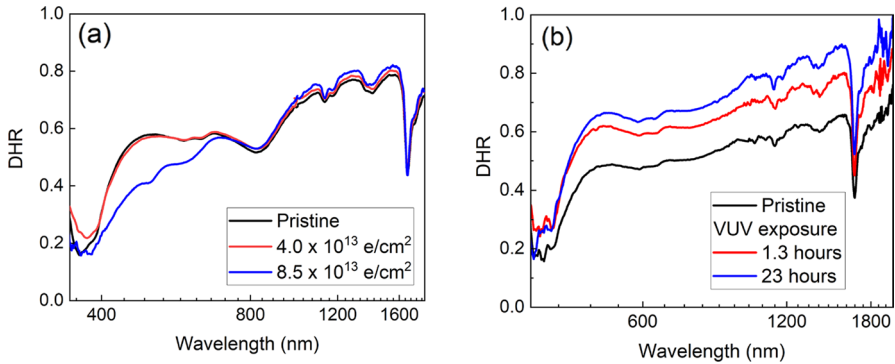
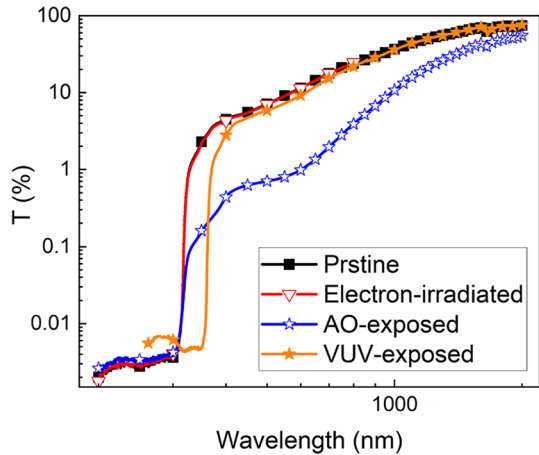


Fig. 5 DHR measurements of **a** electron-irradiated and **b** VUV-exposed Mylar® M021

Fig. 6 Transmission curves of Mylar® M021 material exposed to different components of the space-simulated environment



studied flight duplicate samples; however, results for the AO- and VUV-exposure are still being processed. Figure 9 presents the results of such measurements for pristine and electron-irradiated Mylar® M021 material with 9 mil and 10 mil thicknesses.

Finally, the electrical conductivity of Mylar® M021 was initially planned to be evaluated by two complementary methods, namely, SPD and ASTM D-257. SPD measurements were only partially finished due to hardware issues affecting the material set, and will be presented in a future publication. The ASTM D-257 measurements were completed and are presented in Table 4.

RGB and IR images of Mylar® M021 samples taken during the MISSE-16 orbital experiment. Due to Mylar® M021 (sample #12) being mounted on the swing side of the MCSs alongside three other samples, its imagery on wake and ram MCSs was impacted by a sensor malfunction, leading to the delivery of only the images captured by the zenith MSC during the mission, as shown in Fig. 10. Zenith, oriented toward the space opposite to Earth, receives the highest amount

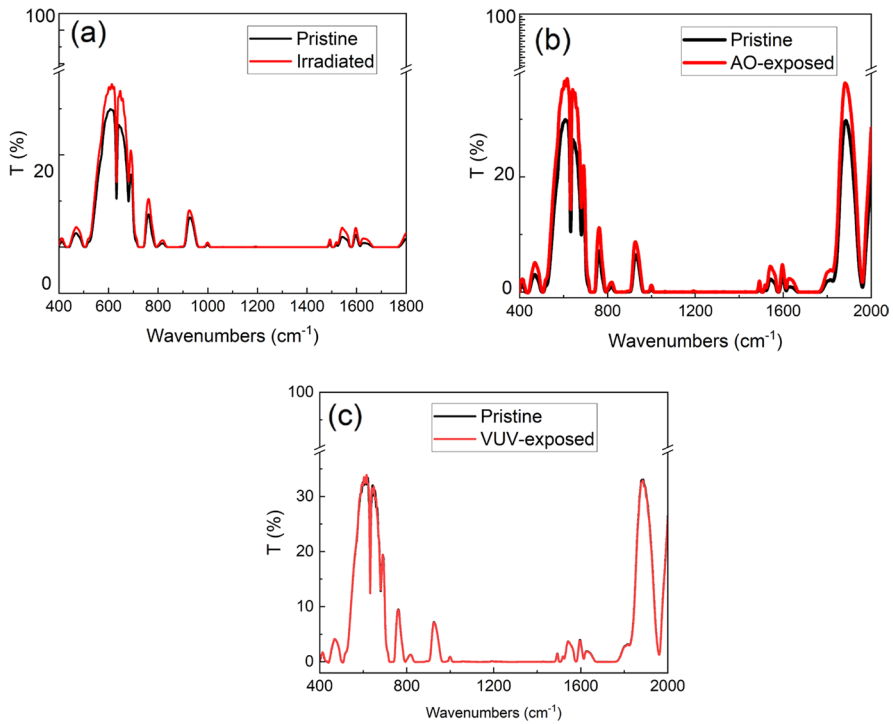
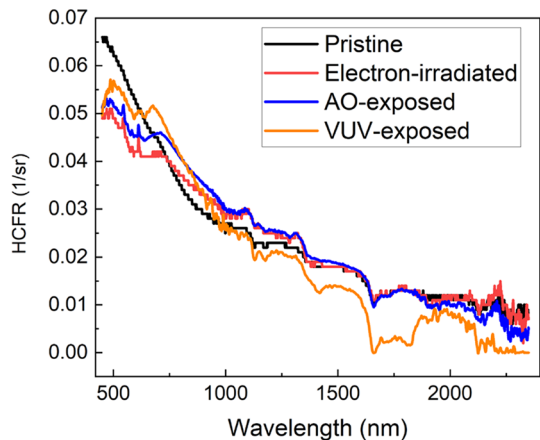


Fig. 7 FTIR Transmission curves of Mylar® M021 material exposed to **a** high energy electrons, **b** AO, and **c** VUV components of the space-simulated environment

Fig. 8 HCFR measurements taken at 0° illumination angle (Θ_i) and 30° viewing angle (Θ_v) of Mylar® M021 material exposed to different damaging types of irradiation



of solar illumination [39]. The respective reflectance values extracted from the zenith RGB pictures taken on orbit during the MISSE-16 mission using ML algorithm are presented in Fig. 11.

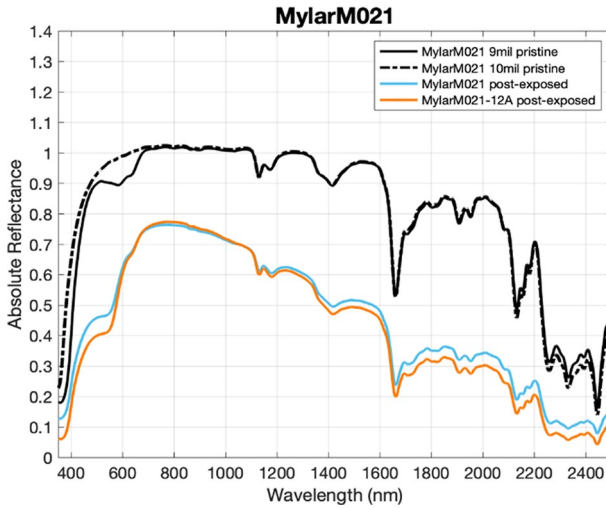


Fig. 9 Absolute reflectance measurements of Mylar® M021 in its pristine state and after electron irradiation. Adapted from [38].

Table 4 Bulk resistivity ($\Omega\text{-cm}$) of Mylar® M021 exposed to different components of space-simulated environment

Material	ASTM D-257		
	100 V	500 V	1000 V
Pristine	3.6×10^{17}	5.6×10^{17}	5.1×10^{17}
Electron-irradiated	1.4×10^{16}	8.4×10^{16}	1.3×10^{17}
AO-exposed	8.3×10^{16}	1.4×10^{17}	1.3×10^{17}
VUV-exposed	2.0×10^{17}	5.7×10^{17}	5.1×10^{17}

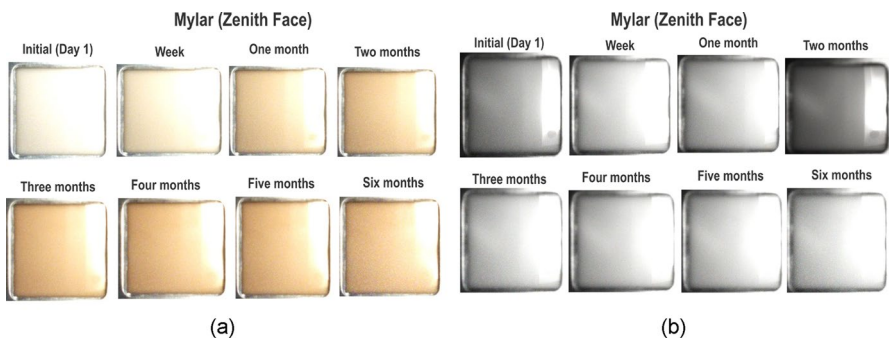
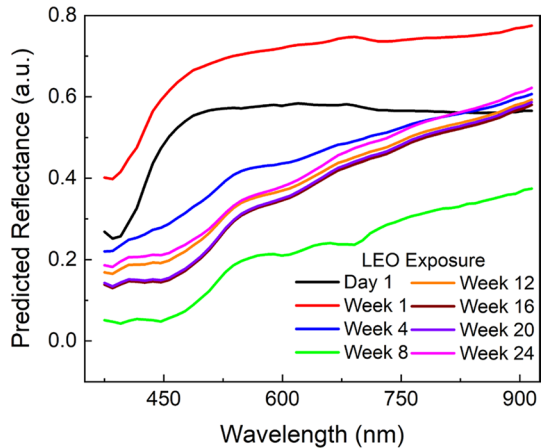


Fig. 10 **a** RGB and **b** IR images of Mylar® M021 delivered from the zenith face of ISS characterized by the predominant VUV exposure. Data were taken during 08/31/22–02/23/23

Fig. 11 Predicted reflectance values of Mylar® M021 extracted from the RGB pictures taken on orbit during the MISSE-16 mission using ML algorithm



4 Discussion

Among three different components of LEO space environment, namely, high energy electron irradiation, AO- and VUV-exposure, the AO irradiation has the most detrimental effect on the surface morphology of the Mylar® M021. Exposure of polymer materials to AO at 8 km/s is sufficient to break the polymer bonds and induce oxidative decomposition, resulting in substantial erosion of polymer surfaces which manifests itself as mass loss, thinning, and texture roughening. AO exposure resulted in an increase of the surface roughness from 7.8 nm (pristine material) to 187.2 nm. Due to the nature of electron and VUV particles we did not expect to reveal significant surface modifications of the electron-bombarded and VUV-exposed samples, which was confirmed by the visual inspection of irradiated materials as well as AFM data. SEM measurements confirmed the erosion of the AO-exposed Mylar® M021. It is noteworthy that both electron irradiation and VUV exposure resulted in a decrease in surface roughness of the material in comparison to the pristine sample. This reduction in surface roughness may indicate an increase in radiation-induced crosslinking.

DHR measurements of the electron-irradiated and VUV-exposed samples revealed the degradation of reflectance after the electron exposure in 400–700 nm region whereas the prolonged VUV exposure (23 h) resulted in increased reflectance values in the entire studied wavelength range (Fig. 5). Absolute reflectance measurements of electron-irradiated Mylar® M021 (Fig. 9) demonstrated a similar trend. Degradation of reflectance after electron bombardment may be attributed to the radiation-induced condensation of aromatic rings into compact carbonaceous clusters [40]. The observed reflectance behavior after VUV exposure may be attributed to the changes in surface microscale smoothness caused by VUV-induced chemical and/or structural changes in polymer surfaces. UV photons are energetic enough to dissociate molecular bonds, resulting in photo-oxidation reactions that scissor or crosslink the polymer chains causing surface morphology modifications. Additional analysis of this PET material as well as similar materials in this class is necessary to

accurately characterize the nature of the chemical changes caused by VUV exposure to PET materials.

The transmission properties of Mylar® M021 material in the 350 nm–2000 nm range were expected to undergo significant degradation following AO exposure, resulting in a complete loss of transparency and an opaque appearance. Oppositely, after high-energy electrons and VUV irradiation, the transmittance of the studied material did not change considerably. Interestingly, that electron and AO exposure did not change the band edge position of the material with respect to its pristine state (~303 nm), whereas VUV exposure caused a shift of the band edge to the ~348 nm, suggesting VUV-exposure induced shrinkage of the bandgap. This bandgap shrinkage may be caused by the presence of excited states and free radicals in the bandgap of the VUV-exposed PET, or, alternatively, by the formation of carbonyl groups and other oxygen-containing species within the polymer matrix which alters the electronic structure of the material.

FTIR measurements showed no new peaks generated after the exposure to the LEO space weather components, suggesting that no new chemical moieties are formed. FTIR spectra of radiation-damaged materials demonstrated slightly increased overall transmission after high energy bombardment and AO exposure. HCRF measurements of irradiated material demonstrated a reduction of signal intensity after VUV exposure.

After electron irradiation, the bulk resistivity of Mylar® M021 was found to have only a minor reduction, which was not significantly affected by exposure to AO or VUV radiation. These results suggest that the electrical properties of this PET variety are stable under the given levels of exposure to the LEO environment components simulated in this study.

Visual inspection of images taken at MSC mounted on the zenith ISS face (Fig. 10a), characterized by dominant VUV exposure, revealed noticeable changes in the appearance of Mylar® M021 in the visible spectral range. The material's color changed from a bright white at the beginning of the experiment (Day 1) to a creamy yellow at the end of the experiment (Month 6), indicating a shift in the material's optical properties. These changes may be attributed to photochemical reactions such as the accumulation of degradation products and discoloration due to exposure to ultraviolet radiation.

No signs of mechanical degradation caused, for example, by micrometeoroid impacts were observed during the experiment (Fig. 10b) indicating that the Mylar® M021 material remained structurally intact under the conditions of the study. However, other forms of mechanical degradation, such as abrasion or fatigue, may have occurred and will be studied upon return of the MISSE-16 experiment to Earth on April–May 2023.

Analysis of RGB pictures taken during the MISSE-16 mission using ML algorithm allowed for the extraction of predicted reflectance values of Mylar® M021 under predominant VUV irradiation. The results presented in Fig. 11 show that the reflectance of Mylar® M021 changed in a complex manner during LEO exposure. Specifically, it increased by factor of two during the first week of LEO exposure, then it steadily decreased during the first two months of exposure, followed by a gradual restoration to a steady value. These results imply that changes in material

reflectance are contingent on several contributing factors, such as alterations in the environment due to ISS maneuvers, background electron irradiation, as well as temperature fluctuations that induce strain and stress within the material. Also, it should be noted that the accuracy of these predicted values may be affected by the quality of the images and the assumptions made by the ML algorithm. Therefore, further research and validation are necessary to fully understand the behavior of Mylar® M021 under VUV irradiation.

5 Conclusions

A comprehensive physical and chemical characterization of both novel and heritage spacecraft materials during simulated space weather experiments is essential for establishing correlation factors between true space exposure and accelerated space weather experiments conducted on ground facilities. This will enable accurate prediction of on-orbit material performance based on laboratory-based testing. Such characterization can provide insights into the underlying mechanisms of material degradation in space and inform the development of more reliable materials for future space missions.

Throughout the project's duration, we conducted a comprehensive analysis of 15 materials representing diverse chemical families, subjecting them to evaluations under both space-simulated conditions and actual space exposure in LEO. In this paper, we have presented our methodology for investigating changes in the optical properties of various spacecraft polymers, scrutinizing their behavior under both true space and space-simulated LEO conditions.

Considering the extensive breadth of our research, which encompassed more than 90 material coupons (including numerous flight-duplicate samples prepared on the ground and 45 samples launched as part of the MISSE-16 mission), it is impractical to provide a detailed overview within a single manuscript. Therefore, we have selected Mylar® M021 as a representative material for the purposes of this paper highlighting our attempts to establish a connection between the changes in optical properties of the spacecraft polymer and the alterations in surface morphology and charge transport properties induced by various components of the space-simulated LEO environment. We intend to focus on elucidating the impact of various space weather elements, including AO, VUV, and high-energy electrons, on studied materials, as well as a comparative analysis of results obtained from both space-exposed samples and flight-duplicate counterparts, in a set of forthcoming publications.

Acknowledgements This work was partially supported by the Georgia Tech Research Institute Independent Research and Development (IRAD). The authors would like to express their gratitude to all colleagues who contributed to this project, including Mr. Rayn Hoffmann, Drs. Jainisha Shah, Miles Bengtson, Alexey Sokolovskiy, and Mrs. Sydney Collman from the SCICL/AFRL (Albuquerque, New Mexico, USA) for preparation of electron-irradiated and VUV-exposed materials, as well as for the characterization of flight duplicate materials with DHR and ASTM D-257 techniques; Drs. Heather Cowardin (NASA) and Jacqueline Reyes (University of Texas at El Paso) for performing absolute reflectance measurements on flight duplicate materials and thorough analysis of their results; Dr. Daniel Engelhart (University of New Mexico) for the valuable insights, expertise, and dedication which were instrumental

in the success of this research endeavor; and Mr. Timothy R. Scott from DuPont de Nemours, Inc, for providing materials for this research.

Disclaimers The views expressed are those of the author and do not necessarily reflect the official policy or position of the Department of the Air Force, the Department of Defense, or the U.S. government. The appearance of external hyperlinks does not constitute endorsement by the United States Department of Defense (DoD) of the linked websites, or the information, products, or services contained therein. The DoD does not exercise any editorial, security, or other control over the information you may find at these locations.

Data availability Not applicable.

Declarations

Conflict of interest On behalf of all authors, the corresponding author states that there is no conflict of interest.

References

1. Star Walk: Astronomical News. <https://starwalk.space/en/news/spacex-starlink-satellites-night-sky-visibility-guide#is-it-ok-to-launch-such-a-large-number-of-starlink-satellites>
2. Lu, Y., Shao, Q., Yue, H., Yang, F.: A review of the space environment effects on spacecraft in different orbits. *IEEE Access* **7**, 93473–93488 (2019)
3. Abd El-Hameed, A.M.: Radiation effects on composite materials used in space systems: a review. *NRIAG J. Astron. Geophys.* **11**(1), 313–324 (2022)
4. de Groh, K.K., Banks, B.A., Miller, S.K., Dever, J.A.: Degradation of spacecraft materials. In: *Handbook of Environmental Degradation of Materials*, pp. 601–645. William Andrew Publishing (2018)
5. Allegri, G., Corradi, S., Marchetti, M., Milinchuk, V.K.: On the degradation of polymeric thin films in LEO space environment. *Mater. Space Environ.* **540**, 255–264 (2003)
6. Awaja, F., Moon, J.B., Gilbert, M., Zhang, S., Kim, C.G., Pigram, P.J.: Surface molecular degradation of selected high performance polymer composites under low earth orbit environmental conditions. *Polym. Degrad. Stab.* **96**(7), 1301–1309 (2011)
7. de Groh, K.K., Banks, B.A.: Atomic oxygen erosion data from the MISSE 2–8 missions (No. NASA/TM—2019–219982) (2019)
8. Yang, J.C., de Groh, K.K.: Materials issues in the space environment. *MRS Bull.* **35**, 12–19 (2010)
9. McTernan, J.K., Bilén, S.G., Krause, L.H.: Facility for real-time test and verification of LEO space plasma phenomena. In: *Applied Space Environments Conference*, Huntsville, AL (2017)
10. Grossman, E., Gouzman, I., Lempert, G., Noter, Y., Lifshitz, Y.: Assessment of atomic-oxygen flux in low-Earthorbit ground simulation facilities. *J. Spacecr. Rocket.* **41**(3), 356–359 (2004)
11. Kleiman, J., Iskanderova, Z., Gudimenko, Y., Horodetsky, S.: Atomic oxygen beam sources: a critical overview. *Mater. Space Environ.* **540**, 313–324 (2003)
12. Dever, J.A., Banks, B.A., de Groh, K.K., Miller, S.K.: Degradation of spacecraft materials. In: Kutz, M. (ed.) *Handbook of Environmental Degradation of Materials*, pp. 465–501. William Andrew Publishing, Norwich (2005)
13. de Groh, K.K., Banks, B.A., Dever, J.A., Jaworske, K.J., Miller, S.K., Sechkar, E.A., Panko, S.R.: NASA Glenn Research Center’s Materials International Space Station Experiments (MISSE 1–7). In: *Proceedings of the International Sym. on “SM/MPAC&SEED Experiment,” JAXA-SP-08–015E*, pp. 91–119 (2009)
14. de Groh, K.K., Banks, B.A.: MISSE-flight facility polymers and composites experiment 1–4 (PCE 1–4). NASA TM-20205008863 (2021)
15. Gold, T.: Lunar-surface closeup stereoscopic photography. *Apollo 14 - Preliminary Science Report*, pp. 272–239 (1969)
16. Ramayanti, S., Budiantoro, P.A., Fauzi, A., Fitrianiingsih, E., Nasser, E.N.: Comparative study of deployable satellite solar panel structure between Carbon Fiber Reinforced Polymer and Al-7075

- Honeycomb. In: 2022 IEEE International Conference on Aerospace Electronics and Remote Sensing Technology (ICARES), pp. 1–6
17. Park, S.Y., Choi, H.S., Choi, W.J., Kwon, H.: Effect of vacuum thermal cyclic exposures on uni-directional carbon fiber/epoxy composites for low earth orbit space applications. *Compos. B Eng.* **43**(2), 726–738 (2021)
 18. Sethi, S., Ray, B.C.: Environmental effects on fibre reinforced polymeric composites: evolving reasons and remarks on interfacial strength and stability. *Adv. Coll. Interface. Sci.* **217**, 43–67 (2015)
 19. Cowardin, H., Seitzer, P., Abercromby, K., Barker, E., Schildknecht, T.: Characterization of orbital debris photometric properties derived from laboratory-based measurements. In: 2010 AMOS Technical Conference No. JSC-CN-21447
 20. White, T.J., Broer, D.J.: Programmable and adaptive mechanics with liquid crystal polymer networks and elastomers. *Nat. Mater.* **14**(11), 1087–1098 (2015)
 21. Campo, E.A.: Complete Part Design Handbook 162. Hanser, Munich (2006)
 22. Gupta, S.: Application of liquid crystals in space activities. In: Prasad, P.N., Nigam, J.K. (eds.) *Frontiers of Polymer Research*, pp. 189–193. Springer, Boston, MA (1991)
 23. Cepeda-Rizo, J., Gayle, J., Ravich, J.: The multilayer insulation (MLI) blanket. In: *Thermal and Structural Electronic Packaging Analysis for Space and Extreme Environments*, pp. 33–40. CRC Press (2021)
 24. Hasan, M.A., Rashmi, S., Esther, A., Bhavanisankar, P.Y., Sherikar, B.N., Sridhara, N., Dey, A.: Evaluations of silica aerogel-based flexible blanket as passive thermal control element for spacecraft applications. *J. Mater. Eng. Perform.* **27**(3), 1265–1273 (2018)
 25. Petroffe, G., Beouch, L., Cantin, S., Chevrot, C., Aubert, P.-H., Dudon, J.-P., Vidal, F.: Thermal regulation of satellites using adaptive polymeric materials. *Sol. Energy Mater. Sol. Cells* **200**, 110035 (2019)
 26. Nikpourian, H., Bahramian, A.R.: Thermo-physical properties of multilayer super insulation: the role of aerogel blanket. *Therm. Sci. Eng. Prog.* **20**, 100751 (2020)
 27. Cooper, S., Hoffman, R.: Jumbo space environment simulation and spacecraft charging chamber characterization. Technical Report Air Force Research Laboratory, Space Vehicles Directorate Kirtland AFB (2015)
 28. Engelhart, D.P., Plis, E., Humagain, S., Greenbaum, S., Ferguson, D., Cooper, R., Hoffmann, R.: Chemical and electrical dynamics of polyimide film damaged by electron radiation. *IEEE Trans. Plasma Sci.* **45**(9), 2573–2577 (2017)
 29. Resonance Ltd.: KrLM-LQD12 lamp comparison. https://resonance.on.ca/index_html_files/LampCmparisonBrochure.pdf
 30. Lean, J.L., Skumanich, A.: Variability of the Lyman alpha flux with solar activity. *J. Geophys. Res. Space Phys.* **88**(A7), 5751–5759 (1983)
 31. Plis, E., Bengtson, M., Engelhart, D.P., Badura, G., Scott, T., Cowardin, H., Reyes, J., Hoffmann, R., Sokolovskiy, A., Ferguson, D., Shah, J., Horne, S.: Characterization of novel spacecraft materials under high energy electron and atomic oxygen exposure. In: *AIAA SCITECH 2022 Forum*, p. 0797 (2022)
 32. Frederickson, A.R., Dennison, J.R.: Measurement of conductivity and charge storage in insulators related to spacecraft charging. *IEEE Trans. Nucl. Sci.* **50**(6), 2284–2291 (2003)
 33. Bengtson, M., Maxwell, J., Hoffmann, R., Cooper, R., Schieffer, S., Ferguson, D., Johnston, W.R., Cowardin, H., Plis, E., Engelhart, D.: Optical characterization of commonly used thermal control paints in a simulated GEO environment. In: *The Advanced Maui Optical and Space Surveillance Technologies Conference*, p. 33 (2018)
 34. Badura, G., Plis, E., Valenta, C.R.: Extending laboratory BRDF measurements towards radiometric modeling of resident space object spectral signature mixing. In: *Advanced Maui optical and space surveillance technologies conference (AMOS)* (2021)
 35. Krech, R.H., Caledonia, G.E.: Novel oxygen atom source for material degradation studies. Final report, 1 March 1986–1 September 1988. Physical Sciences, Inc., Andover, MA (United States) (1988)
 36. Collman, S., Plis, E.A., Shah, J.R., Bengtson, M.T., Hoffmann, R.C., Ferguson, D.C.: Operational procedure for handling of spacecraft materials sensitive to atmospheric exposure. *J. Spacecr. Rockets* **60**(2), 685–688 (2023)
 37. Nguyen, R.M., Prasad, D.K., Brown, M.S.: Training-based spectral reconstruction from a single RGB image. In: Fleet, D., Pajdla, T., Schiele, B., Tuytelaars, T. (eds.) *Computer Vision – ECCV*

2014. ECCV 2014. Lecture Notes in Computer Science, vol. 8695, pp. 186–201. Springer, Cham (2014)
38. Cowardin, H., Reyes, J., Plis, E.A., Hoffmann, R.C., Badura, G.P., Shah, J.R., Collman, S.E.J., Bengtson, M.T., Engelhart, D.P.: Spectral characterization of modern spacecraft materials. In: Advanced Maui Optical and Space Surveillance Technologies Conference (AMOS) (2022)
 39. Snow, K.E., de Groh, K.K., Banks, B.A., Sechkar, E.A.: Bend-test results of the MISSE 7 flexural stress effects experiment after 1.5 years of space exposure (No. GRC-E-DAA-TN62672) (2019)
 40. Steckenreiter, T., Balanzat, E., Fuess, H., Trautmann, C.: Chemical modifications of PET induced by swift heavy ions. Nucl. Instrum. Methods Phys. Res., Sect. B **131**(1–4), 159–166 (1997)

Publisher's Note Springer Nature remains neutral with regard to jurisdictional claims in published maps and institutional affiliations.

Springer Nature or its licensor (e.g. a society or other partner) holds exclusive rights to this article under a publishing agreement with the author(s) or other rightsholder(s); author self-archiving of the accepted manuscript version of this article is solely governed by the terms of such publishing agreement and applicable law.